Available online at www.sciencedirect.com
SCIENCE DIRECT
Catalysis Today 113 (2006) 245–250
CATALYSIS TODAY
www.elsevier.com/locate/cattod

Structural properties of CoPt films patterned using ion irradiation

M. Abes [a], J. Venuat [a], D. Muller [b], A. Carvalho [a], G. Schmerber [a], E. Beaurepaire [a], A. Dinia [a], V. Pierron-Bohnes [a,*]

[a] IPCMS-GEMME (UMR 7504 CNRS), ULP-ECPM, 23 rue du Loess BP 43 67034 Strasbourg Cedex 2, France
[b] Laboratoire PHASE, (UPR 292 CNRS), 23 rue du Loess, 67037 Strasbourg Cedex, France

Available online 19 January 2006

Abstract

Patterned CoPt films were fabricated using a combination of e-beam lithography and He^+ ion irradiation to produce a planar array of ordered CoPt squares separated by disordered CoPt areas: (i) by molecular beam epitaxy was deposited a CoPt ordered film which corresponds to a ''natural'' multilayer: alternating pure cobalt and pure platinum (0 0 1) planes. (ii) The film was covered by a 300 nm thick Pt layer mask. (iii) Irradiation with appropriate ion beam and fluence disorders the CoPt film where not protected by the mask. X-ray diffraction, as well as atomic and magnetic force microscopy, is used to characterise the structural and magnetic changes in the film. The He^+ ion irradiation does not significantly modify the surface of the CoPt film: the roughness almost remains identical (~2 nm). This is promising for applications in magnetic recording technologies.

PACS: 75.30.Gw; 75.50.Ss; 75.60.Ej; 61.80.Jh

Keywords: Structural properties; Roughness; CoPt films; Magnetic properties; Ion irradiation

Areal density enhancement is a major challenge in magnetic recording because of magnetization thermal fluctuations of superparamagnetic grains when their size is below a critical value [1]. High anisotropy patterned media could be a promising response to this problem [2]. However, surface roughness will likely deteriorate the signal to noise ratio. A critical planarization step is thus required at the end of the process to obtain medium compatibility with low altitude reading.

Light ion (He^+) irradiation have been shown to modify in a precisely controlled way the structural and magnetic properties of Co/Pt multilayers or FePt alloys, through chemical mixing [3–6], with negligible change of surface roughness. More recently, we have shown that light ion irradiation can induce the chemical disorder in CoPt alloy layers [7]. The CoPt alloy layers are deposited on a MgO(0 0 1) substrate at 900 K by molecular beam epitaxy or by sputtering. These conditions favor the $L1_0$ chemically ordered phase. Their structure is based on a face centered cubic (fcc) lattice with pure M (Co or Fe) and P (Pt or Pd) planes stacked along the [0 0 1] direction (*c*-axis), producing a tetragonal distortion along this direction. Irradiation of ordered CoPt films with 40 keV He^+ ions at room temperature breaks chemical order, due to irradiation induced atomic displacements. The He^+ ion irradiation is known to induce two main mechanisms in metals: (i) the enhancement of the atomic diffusion due to the energy deposited through the interaction of the ions with the electronic distribution (equivalent to a temperature enhancement and to an annealing of the sample; this can help the alloy to perfect its order state, nevertheless the local transition temperature can be higher than the order–disorder temperature of the alloy, which will have the effect to disorder it along the ion trajectories), (ii) the ballistic effect due to the collisions of the alloy species with the He^+ ions, which induces Co and Pt atoms move away from their initial positions (and break the order of the alloy). The disordering mechanisms seem more efficient in the CoPt system than in the FePt system [6], certainly because the order–disorder temperature is quite low in this system (1100 K) and the driving force for ordering is quite small. This effect is believed to drive the observed changes [7], since the magnetic anisotropy is very sensitive to local atomic rearrangement. However, ionic irradiation can be favorably used to pattern magnetic films [8], by using appropriate mask to protect some

* Corresponding author. Tel.: +333 88 10 70 73; fax: +333 88 10 72 49.
E-mail address: vero@ipcms.u-strasbg.fr (V. Pierron-Bohnes).

0920-5861/$ – see front matter © 2005 Elsevier B.V. All rights reserved.
doi:10.1016/j.cattod.2005.11.087

nano-elements of the film, while others are exposed to ionic irradiation. The irradiated regions will thus become magnetically soft whereas the protected regions will remain magnetically hard. Thus, for data storage applications, the information could be stored as perpendicular bits in the non-irradiated regions. This method could have a great impact on the current race toward high anisotropy materials to increase magnetic recording density.

We present here the structural properties of such nanostructured materials, a planar array of ordered CoPt squares separated by disordered CoPt areas. We also discuss the influence of irradiation on both the surface and the order state in the patterned CoPt film.

1. Experimental procedure

The ordered CoPt thin films were grown at 900 K by MBE in a ultrahigh vacuum chamber [9]. The samples consist of a 50 nm thick epitaxial $Co_{50}Pt_{50}$ layer, grown on a MgO(0 0 1) substrate degassed for 12 h at 1000 K. Using the flux and temperature co-deposition conditions previously optimized in this system [9], a single variant $L1_0$ ordered phase has been obtained with the concentration modulation perpendicular to the surface. All samples were covered at room temperature by a 5 nm thick Pt capping layer to prevent oxidation.

Irradiation was carried out with a conventional ion implanter. The irradiation parameters were chosen from previous results [7]. In order to obtain low and uniform energy deposit in the films, we used He^+ ions of energy 40 keV. According to transport and ranges of ions in matter (TRIM) simulations, the number of displaced atoms in the CoPt layer is about 2×10^{-3} per incoming ion and per nanometer. A fluence of 6×10^{16} ions/cm^2 is used at a low current density to avoid any heating of the sample. He^+ ions are stopped in the MgO substrate after irradiation.

The sputtering phenomenon during the irradiation can deteriorate the surface flatness a priori. By atomic force microscopy, we observed the surface quality of the CoPt film before (Fig. 1a) and after irradiation (Fig. 1b) and noted that the He^+ ion irradiation does not significantly modify the surface of the sample. Roughness remains almost identical (~2 nm). This negligible deterioration of the surface is in agreement with the weak yield of pulverization calculated by TRIM ($Y = 0.04$ atoms/He^+ ion, i.e. 0.4 nm for 10^{17} He^+/cm^2).

A Pt mask was deposited in order to protect some parts of the sample from irradiation. A sacrificial 50 nm Cu layer was deposited before the Pt mask, to allow chemical removing of the array after irradiation [10]. The mask was fabricated by electron-beam photoresist lithography with a 800 nm thick layer of [poly(methylmethacrylate) (PMMA)–methacrylic acid (MAA)] co-polymer resist covered by a standard 950 K PMMA resist (thickness 100 nm). Exposures were made using a JEOL 840 e-beam microscope equipped with a Raith's pattern generator [11], operating at 35 kV and with a beam current of 100 pA. The 300 nm thick Pt film was deposited on the nanostructured resist. After the lift-off, we obtained 1 μm^2 square-shaped Pt dots, separated by 1 μm (Fig. 2).

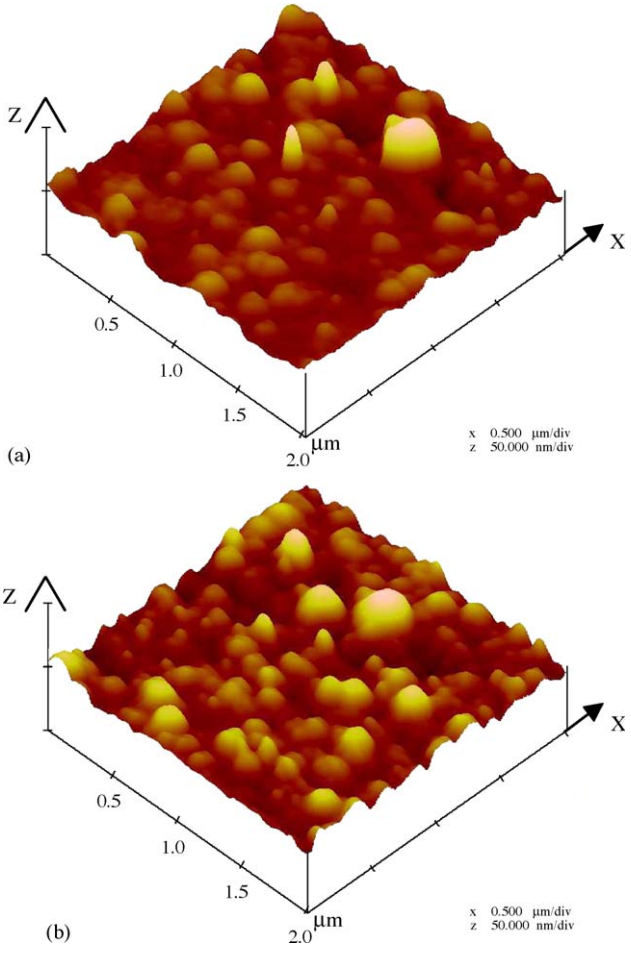

Fig. 1. Topographic images obtained by AFM on the surface of a CoPt layer before (a) and after He^+ ion irradiation with a fluence of 6×10^{16} ions/cm^2 (b). The image size is 2 μm × 2 μm.

X-ray diffraction measurements were performed on a D-500 Siemens diffractometer with a monochromatic Co $K\alpha_1$ incident beam ($\lambda = 0.17889$ nm). ω-2θ reflection scans and rocking curves in symmetrical and asymmetrical geometries were collected (ω is the incident angle) in order to (i) measure the crystalline quality of the layer, (ii) have access to the long-range order state, and (iii) test the presence of other variants. Using a home-made sample holder with a rotation axis in the diffraction plane, we have optimized the diffracted intensity versus the orientation of the sample around both axes in its plane to be able to compare the peak intensities before and after irradiation.

Atomic and magnetic force microscopy (AFM and MFM) images were obtained using a Nanoscope III from Digital Instruments.

2. Results

Reflection high energy electron diffraction (RHEED) images, realized during the deposition along the [0 1 0] azimuth, allow us to have a first estimation of the crystalline growth quality of the CoPt layer (Fig. 3). On this image, the thin lines are characteristic of a good crystalline quality and a weak roughness. We clearly see the [−2 0 0] and [2 0 0] diffraction

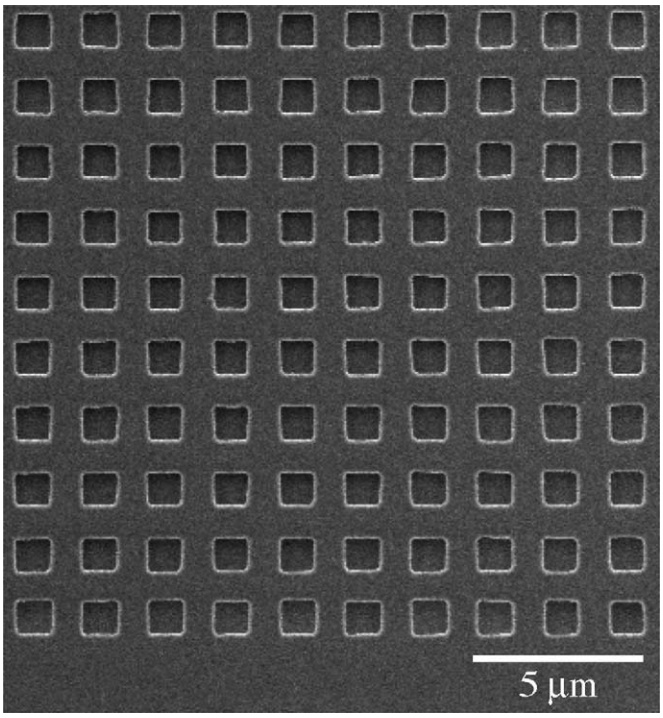

Fig. 2. Scanning electron microscopy image of 300 nm thick Pt dots (1 µm × 1 µm) after lift-off.

lines, which characterize the epitaxial growth of the layer on the MgO(0 0 1) substrate.

The optimal thickness of the mask was determined irradiating ordered CoPt layers with a continuous Pt capping of different thickness. The structural modifications in the films were studied using X-ray diffraction before and after

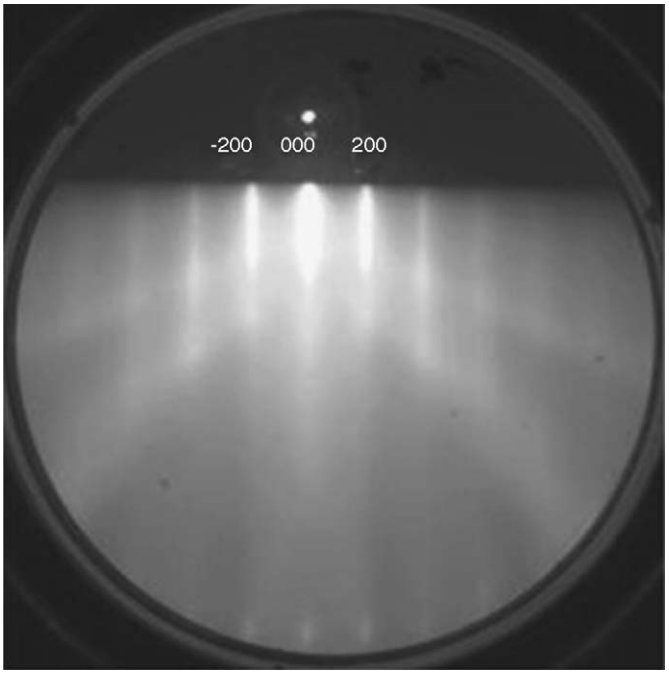

Fig. 3. RHEED photo on the CoPt surface realized along the [0 1 0] azimuth during the deposit.

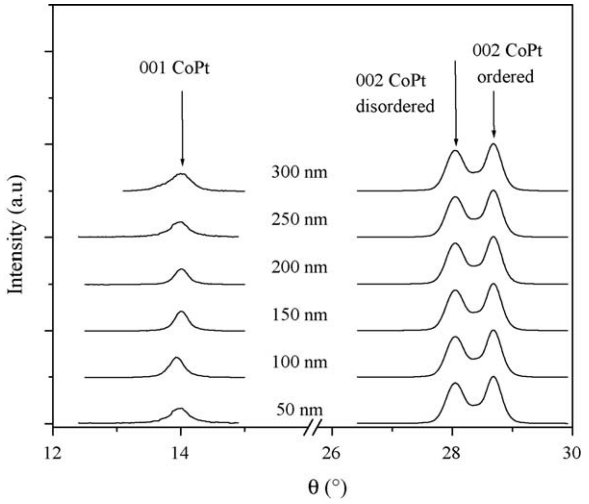

Fig. 4. θ–2θ scans before irradiation around the 0 0 1 superstructure peak and the 0 0 2 fundamental peak for ordered CoPt layers with a Pt capping of different thickness (λ = 0.17889 nm).

irradiation. The spectra in Figs. 4 and 5 clearly show a change in structural and chemical order, due to the irradiation process, for the CoPt layers with a Pt capping of thickness smaller than 200 nm.

Before irradiation, besides the 0 0 2 MgO substrate peak (not shown here), different diffraction peaks corresponding to the CoPt alloy film are distinctly observed: the 0 0 2 fundamental peak is present (Fig. 4), as well as the 0 0 1 superstructure line characteristic of the CoPt $L1_0$ ordered phase (Fig. 4). The 0 0 2 fundamental peak divides in two peaks. The high angle 0 0 2 peak belongs to the disordered phase and the low angle 0 0 2 peak belongs to the $L1_0$ ordered phase, since its position corresponds to the 0 0 1 superstructure peak position. Concentration fluctuations during the deposition may be explain the presence of this high angle 0 0 2 fundamental peak of the CoPt film. Its position corresponds to the *A*1 disordered phase with a 40% cobalt concentration.

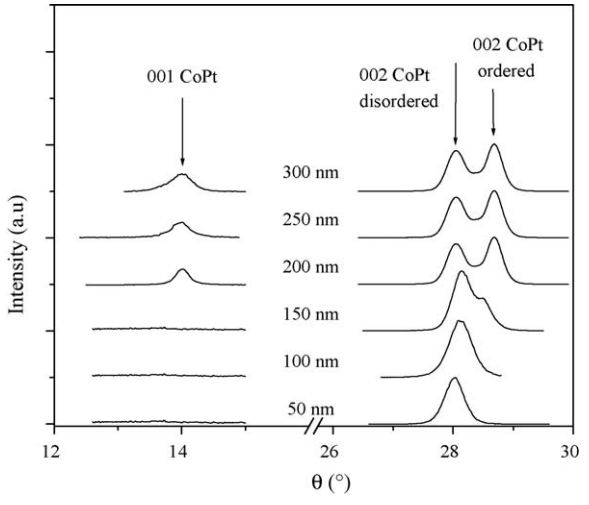

Fig. 5. θ–2θ scans after irradiation around the 0 0 1 superstructure peak and the 0 0 2 fundamental peak for ordered CoPt layers with a Pt capping of different thickness (λ = 0.17889 nm).

The perfect CoPt $L1_0$ phase can be described as a stacking of pure Co and pure Pt (0 0 1) planes defining two sublattices (α, β). This chemical order is accompanied by a tetragonalization of the cubic cell with c, the lattice parameter along the [0 0 1] concentration modulation direction, 4% smaller than a, the lattice parameter in the other directions [12].

The $L1_0$ equilibrium phase can present three variants because there are three directions equivalent to [0 0 1] in the fcc: the concentration modulation can occur along the [1 0 0] and [0 1 0] directions in the plane, or in the [0 0 1] direction perpendicular to the surface of the sample. The latter variant give rise to the 0 0 1 superstructure peak observed with the scattering vector along the surface normal. ω-2θ reflection scans in the asymmetrical geometry have shown that 1 0 2 and 0 1 2 superstructure peaks, corresponding, respectively to [1 0 0] and [0 1 0] variants, are absent. This shows that the ordering is unidirectional during the growth.

For the CoPt layers with a Pt capping of thickness smaller than 200 nm (Fig. 5), the 0 0 1 superstructure and 0 0 2 fundamental peaks corresponding to the $L1_0$ ordered phase disappear with the irradiation. This shows that a 200 nm thick Pt capping is sufficient to protect the CoPt film from the He^+ ion irradiation.

In partially $L1_0$-ordered Co_xPt_{1-x} samples, the degree of $L1_0$ order is usually described by the LRO parameter η defined as $\eta = |x_\alpha - x_\beta|/(1 - |1 - 2x|)$, where $x_{\alpha(\beta)}$ is the Co concentration in the $\alpha(\beta)$ sublattice (the denominator ensures $\eta = 1$ for the highest order, even out of stoichiometry). η can be deduced from the relative intensities of a superstructure Bragg peak I_S compared to a fundamental peak intensity I_F by the following relation:

$$\eta^2 = \frac{I_S}{I_F}\frac{4\bar{F}^2}{\Delta F^2(1-|1-2x|)^2}\frac{\exp(B_S \sin^2\theta_S/\lambda^2)}{\exp(B_F \sin^2\theta_F/\lambda^2)} = C\frac{I_S}{I_F} \quad (1)$$

where $\bar{F} = xF_{Co} + (1-x)F_{Pt}$ is the average diffusion factor of the CoPt alloy at the fundamental peak position, $\Delta F = F_{Pt} - F_{Co}$ the diffusion factor contrast at the superstructure peak position, $B_S(B_F)$ the Debye–Waller (D–W) attenuation factors [9] associated with the superstructure (fundamental) peaks at room temperature and λ the monochromatic Co radiation wavelength (0.17889 nm). The relative intensities of the superstructure and fundamental peaks have been obtained from the integrated θ–2θ curves (A_S and A_F for the superstructure and fundamental peaks, respectively), the width of the rocking curves (L_S and L_F for the superstructure and fundamental peaks, respectively) and the usual polarization and Lorentz corrections ($LP_{S(F)}$) using the following formula:

$$I_{S(F)} = A_{S(F)}L_{S(F)}\frac{\sin\theta_{S(F)}\sin 2\theta_{S(F)}(1+\cos^2 2\beta)}{1+\cos^2 2\beta\cos^2 2\theta_{S(F)}} = A_{S(F)}L_{S(F)}LP_{S(F)} \quad (2)$$

where β is the reflection angle of the beam on the monochromator and $\theta_{S(F)}$ the positions of the superstructure and fundamental peaks, respectively, in the θ–2θ scans.

Hereafter, we will distinguish η_z the order parameter within the z-variant (normalization to the fundamental peak corresponding to the z-variant) and S_z the apparent order parameter for the z-variant (normalization to the total fundamental peak). When the 0 0 2 fundamental peak can be decomposed into its two components (the z-variant and disordered components), η_z is deduced from relations (1) and (2):

$$\eta_z^2 = C\frac{I_{Sz}}{I_{Fz}} \quad (3)$$

where I_{Sz} and I_{Fz} are the integrated intensities of the superstructure and fundamental peaks corresponding to the z-variant.

On the other hand, when the 0 0 2 fundamental peak cannot be decomposed into its two components, only the apparent order parameter, S_z, can be deduced from:

$$S_z^2 = C\frac{I_{Sz}}{\sum_i I_{Fi}} \quad (4)$$

where $\sum_i I_{Fi}$ is the total integrated intensity of the fundamental peak without decomposition.

When possible, the 0 0 2 fundamental peak was adjusted by a sum of two Gaussian peaks, the z-variant corresponding to the large angle peak and the disordered phase to the small angle peak. The initial apparent long-range order parameter is 0.42 ± 0.1. This value may be an under-estimation because there may be some antiphase boundaries that diminish the average superstructure peak intensity without strongly affecting the chemical short-range order. After irradiation, we get values between 0.45 and 0.0 ± 0.1, depending on the Pt protection thickness. As shown in Fig. 6a, a 200 nm thickness is necessary to protect the film against irradiation of He ions, from the point of view of long range order. As shown in Fig. 6b, a 250 nm thickness is necessary to protect the film against irradiation of He ions, from the point of view of magnetic anisotropy. The variation of the magnetic anisotropy after irradiation with the thickness of the Pt protection is less rapid than the variation of the long-range order parameter. This is due to the magnetic effect of residual short-range order. The comparison of these results with the energy deposit deduced from TRIM simulations (Fig. 6c) clearly shows that it is not possible to predict the disordering effects using TRIM simulations, as the number of jumps necessary to get a disordered phase at short distance is not well known. The long-range order is totally destroyed for a deposited energy smaller than 30 eV/atom/nm, whereas a consequent short-range order is still present for this deposited energy. Fig. 7 present the energy losses yielded to the Co and Pt atoms in the CoPt layer for different thicknesses of Pt. The effective energy necessary to move the atoms is equal to 0.5 eV/Å/ion. According to TRIM, for a thickness higher than 200 nm, the ions are not able to move any atom in the CoPt layer (Fig. 7c). To have a safety margin, we chose to deposit a 300 nm thick mask.

The spectra of X-ray diffraction corresponding to the film irradiated through the mask (c) (containing both irradiated and non-irradiated regions) is qualitatively a linear combination of the spectra from the ordered and disordered chemically regions corresponding to completely protected (a) and non protected (b)

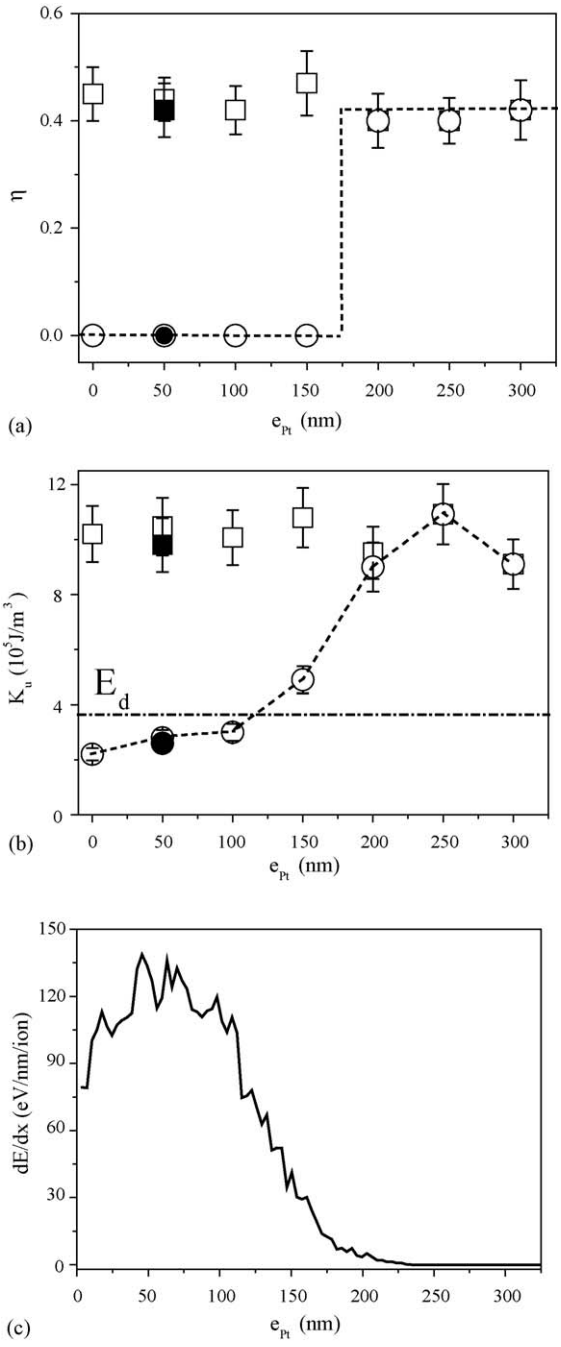

Fig. 6. (a) Long-range order parameter η and (b) magneto-crystalline anisotropy K_U as a function of the Pt protection layer thickness for a CoPt film before (□) and after (○) He^+ irradiation. The dashed line is a guide for the eye. η drops dramatically after irradiation for a Pt layer thickness smaller than 200 nm and is constant above this value. K_U shows a smoother decrease and becomes smaller than E_d (demagnetizing anisotropy energy) for a thickness larger than 150 nm. The filled symbols correspond to a film capped with only 50 nm of Cu. (c) Deposit energy dE/dx in platinum deduced using the TRIM simulation.

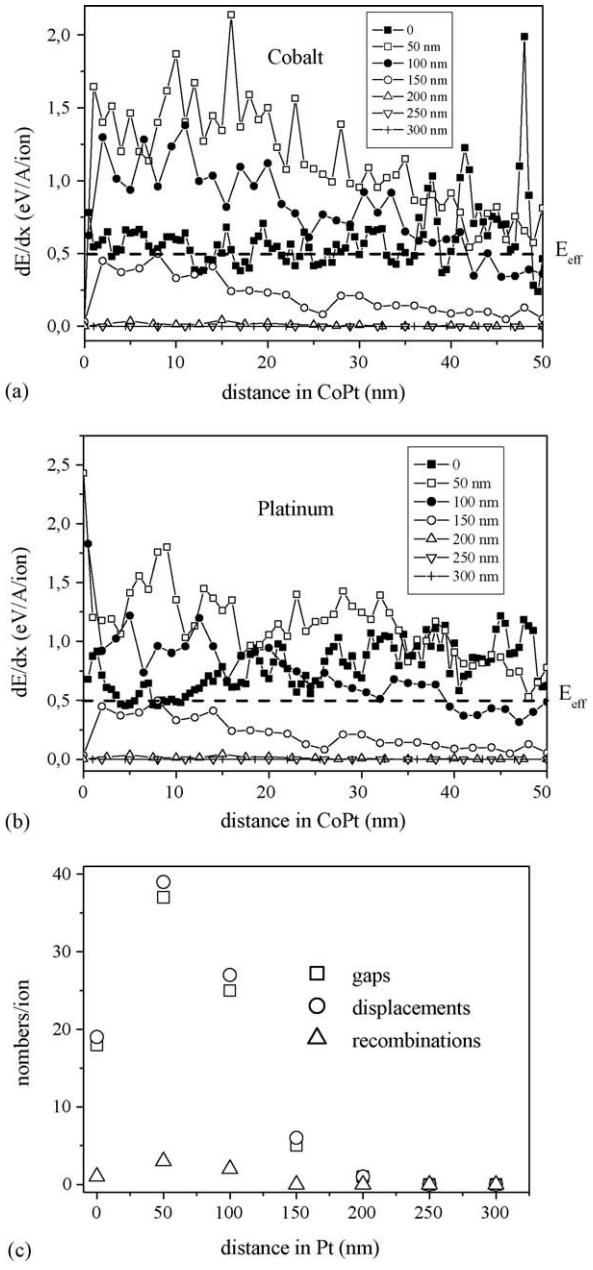

Fig. 7. Energy losses yielded to the cobalt (a) and to the platinum (b) atoms in the CoPt layer as a function of the Pt thickness. The feature in dotted line located at 0.5 eV/Å/ion corresponds to the effective energy to move the Pt and Co atoms in the CoPt layer according to TRIM simulations. (c) Numbers of displacements, of gaps and of recombinations per ion in the CoPt layer as a function of the Pt thickness according to TRIM simulations.

regions, respectively (Fig. 8). S_z and η_z have almost the same value before and after irradiation in the region protected by the mask ($S_z \approx 0.44$ and $\eta_z \approx 0.58$).

We have studied the irradiation effect on the surface quality and on the magnetic configuration in the CoPt film by AFM and MFM. The Pt mask was eliminated to allow a correct AFM and MFM imageries (by a chemical attack of the Cu layer deposited between the CoPt and Pt layers). Fig. 9 shows that the film surface remains quite plane. Fig. 10 shows the MFM image of the CoPt patterned film. The image has been obtained in a perpendicularly demagnetized state after saturating the sample into a 1.7 T field perpendicular to the film surface. This image displays highly interconnected stripes in the protected regions corresponding to up and down orientations of the magnetization. This pattern is similar to those observed in [0 0 1]-oriented $L1_0$ FePd thin films [13]. Spatially-selective irradiation gives

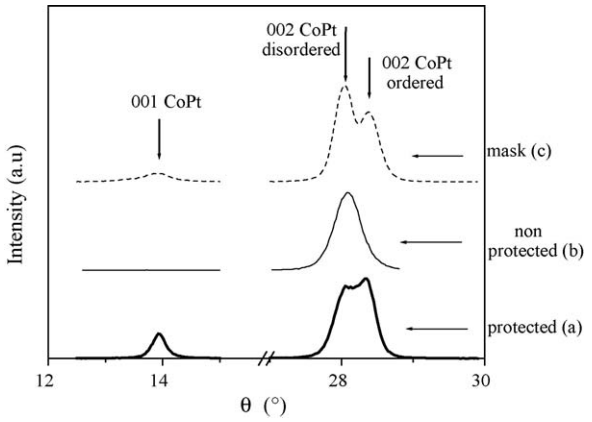

Fig. 8. θ–2θ scans around the 0 0 2 fundamental peak and the 0 0 1 superstructure peak for CoPt layers obtained on three different areas of the CoPt film (completely protected by a 300 nm thick Pt layer, not protected or protected by the 300 nm thick mask) ($\lambda = 0.17889$ nm).

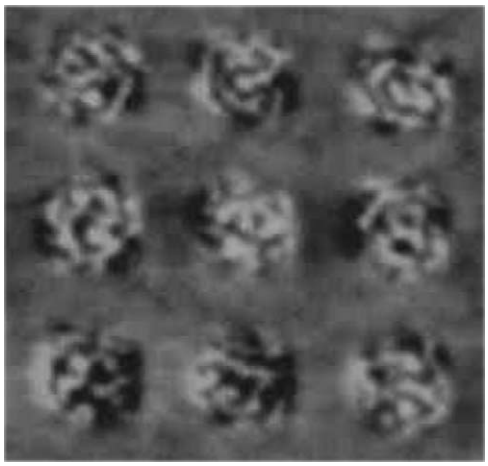

Fig. 10. MFM image of a CoPt film patterned by ion irradiation. The magnetic image has been obtained in perpendicular demagnetized state. The image size is 5.4 μm × 5.4 μm.

rise to a spatial distribution of magnetic anisotropy and hence of the magnetization direction (perpendicular-to-plane in the ordered zones and in-plane in the disordered zones). Moreover, the MFM image shows not well defined contours of the dots. This can be attributed to the fact that the irradiation creates cascades of displacements within a pear-shaped region under the surface thus also partially disordering the borders of the protected areas. A simulation using the TRIM software shows that, due to the Cu layer, these cascades penetrate into the protected regions at lateral distance up to 100 nm. The outer boundaries of the dots are thus partially disordered.

For data storage applications, the data could be stored as perpendicular bits in the non-irradiated regions, which are magnetically hard, although for applications the feature size must clearly be much smaller. We have observed via Atomic Force Microscopy (AFM) that the roughness is only slightly increased by the whole process (2 nm, mainly due to the chemical attack that eliminates the mask). The main interest to use irradiation for nanostructure fabrication is thus that the film remains flat.

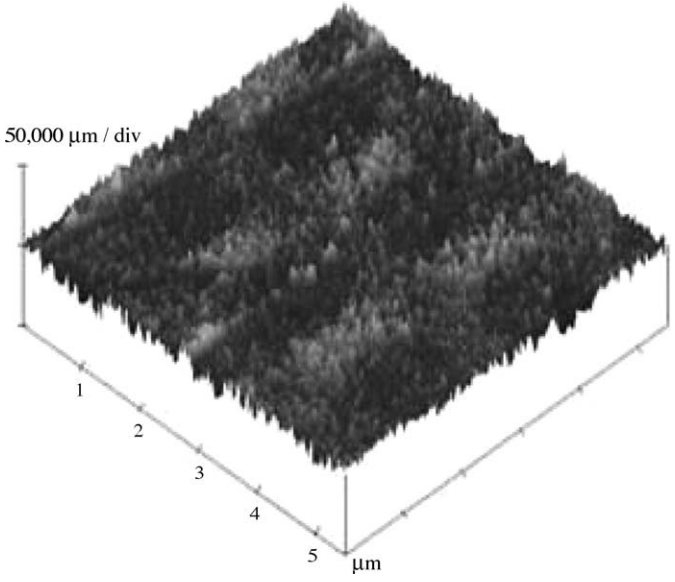

Fig. 9. AFM image of a CoPt film patterned by ion irradiation. The surface roughness of the CoPt film is about 2 nm. The image size is 5.4 μm × 5.4 μm.

References

[1] R.L. White, J. Magn. Magn. Mater. 209 (2000) 1.
[2] S.Y. Chou, Proc. IEEE 85 (1997) 652.
[3] C. Chappert, H. Bernas, J. Ferré, V. Kottler, J.P. Jamet, Y. Chen, E. Cambril, T. Devolder, F. Rousseaux, V. Mathet, H. Launois, Science 280 (1998) 1919;
T. Devolder, C. Chappert, Y. Chen, E. Cambrill, H. Bernas, J.P. Jamet, J. Ferré, Appl. Phys. Lett. 74 (1999) 3383;
T. Devolder, Phys. Rev. B 62 (2000) 5784;
T. Devolder, H. Bernas, D. Ravelosona, C. Chappert, S. Pizzini, J. Vogel, J. Ferré, J.P. Jamet, Y. Chen, V. Mathet, Nucl. Instrum. Methods Phys. Res. B 175 (2001) 375.
[4] G.J. Kusinski, K.M. Krishnan, G. Denbeaux, G. Thomas, B.D. Terris, D. Weller, Appl. Phys. Lett. 79 (2001) 2211;
B.D. Terris, L. Folks, D. Weller, J.E.E. Baglin, A.J. Kellock, H. Rothuizen, P. Vettiger, Appl. Phys. Lett. 75 (1999) 403;
C.T. Rettner, S. Anders, J.E.E. Baglin, T. Thomson, B.D. Terris, Appl. Phys. Lett. 80 (2002) 279.
[5] J.M. MacLaren, R.H. Victora, Appl. Phys. Lett. 66 (1995) 3377.
[6] D. Ravelosona, C. Chappert, V. Mathet, H. Bernas, Appl. Phys. Lett. 76 (2000) 236.
[7] M. Abes, O. Ersen, D. Muller, M. Acosta, C. Ulhaq-Bouillet, A. Dinia, V. Pierron-Bohnes, Mater. Sci. Eng. C 23 (2003) 229.
[8] B.D. Terris, D. Weller, L. Folks, J.E.E. Baglin, A.J. Kellock, H. Rolhvizen, P. Veltiger, J. Appl. Phys. 87 (2000) 7004.
[9] O. Ersen, V. Parasote, V. Pierron-Bohnes, M.C. Cadeville, C. Ulhaq-Bouilllet, J. Appl. Phys. 93 (2003) 2987.
[10] A. Carvalho, M. Geissler, H. Schmid, B. Michel, E. Delamarche, Langmuir 18 (2002) 2406.
[11] Raith Elphy Quantum Universal SEM Nanolithography System, Version 2.07, October 2000, Germany.
[12] C. Leroux, M.C. Cadeville, V. Pierron-Bohnes, G. Inden, F. Hinz, J. Phys. F: Met. Phys. 18 (1988) 2033.
[13] V. Gehanno, A. Marty, B. Gilles, Y. Samson, Phys. Rev. B 55 (1997) 12552.